Convection in vibrated annular granular beds

R. D. Wildman,[1] T. W. Martin,[1] P. E. Krouskop,[2] J. Talbot,[2] J. M. Huntley,[1] and D. J. Parker[3]
[1]*School of Mechanical and Manufacturing Engineering, Loughborough University, Loughborough, Leicestershire LE11 3TU, United Kingdom*
[2]*School of Chemistry and Biochemistry, Duquesne University, Pittsburgh, Pennsylvania 15282 USA*
[3]*School of Physics and Astronomy, University of Birmingham, Edgbaston, B16 2TT, United Kingdom*
(Received 1 October 2004; published 14 June 2005)

The response to vibration of a granular bed, consisting of a standard cylindrical geometry but with the addition of a dissipative cylindrical inner wall, has been investigated both experimentally (using positron emission particle tracking) and numerically (using hard sphere molecular dynamics simulation). The packing fraction profiles and granular temperature distributions (in both vertical and horizontal directions) were determined as a function of height and distance from the axis. The two sets of results were in reasonable agreement. The molecular dynamics simulations were used to explore the behavior of the granular bed in the inner wall–outer wall coefficient of restitution phase space. It was observed that one could control the direction of the toroidal convection rolls by manipulating the relative dissipation at the inner and outer walls via the coefficients of restitution, and with several layers of grains it was seen that double convection rolls could also be formed, a result that was subsequently confirmed experimentally.

DOI: 10.1103/PhysRevE.71.061301 PACS number(s): 45.70.Mg

I. INTRODUCTION

The analogy between rapidly flowing granular materials and some of the more usual states of matter, such as gases and liquids, has been developed over a period of several decades [1]. Working from a microscopic viewpoint, kinetic theory concepts have been extended from non- and near-equilibrium studies of gases and modified to take into account the dissipation during collisions that sets granular materials apart from thermal systems [2–4]. A striking feature of fluidized granular beds is that one may see evidence of instabilities reminiscent of those observed in liquids. For example, recent experimental, numerical and theoretical studies have all pointed towards "thermally" induced convection being a phenomenon closely related to buoyancy driven flows such as Rayleigh-Benard convection and related effects [5–7]. On one level, the physical mechanism driving granular thermal convection is essentially that seen in thermal fluids: buoyancy forces induce differential motion and force convection. In granular systems, however, the granular temperature cannot be given as a boundary condition; it is the dissipation inherent in the system that results in granular temperature gradients and hence, convection. In a vibrated bed for example, one sees that, in general, the system is "hotter" near the base and that it is "cooler" at higher altitudes, due to the dissipation during collisions [8–10]. This has the effect that as we increase the number of particles, or increase the dissipation during the collisions, the temperature gradient becomes steeper, leading to instability in the system [7]. These instabilities have been the subject of a number of studies and have led to the investigation of "symmetry-breaking" phenomena where spontaneous (and seemingly stable) large-scale variations in density occur [11,12].

In numerical simulations of a two-dimensional system, Ramirez *et al.* [5], demonstrated that granular beds could show signs of thermal convection. They suggested that dissipation plays the role of an order parameter for the instability: once a threshold value of the dissipation has been reached, the system appears to undergo a supercritical transition and the convection rolls form. This presence of convection in a three-dimensional system was subsequently confirmed experimentally [6] and good agreement with these results was obtained using a molecular dynamics simulation, developed by Talbot and Viot [13]. The latter study also showed that the strength and direction of the convection roll is strongly influenced by the value of the particle-wall coefficient of restitution.

In Ref. [13] it was suggested that inserting an inner (solid) cylinder coaxial with the outer cylinder might modify the convection pattern. The additional boundary present in this configuration is expected to allow greater control over the

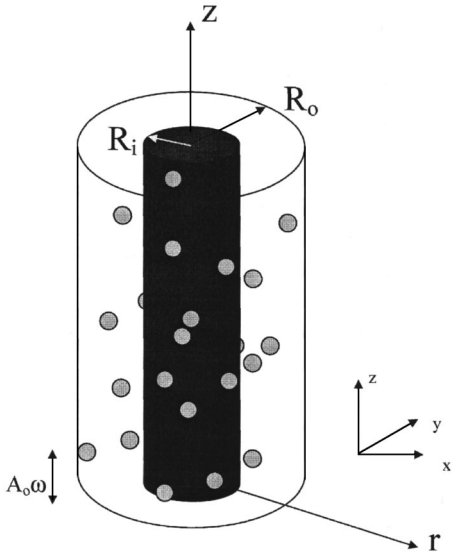

FIG. 1. Schematic of cell geometry, showing an annular cell system that is vibrated from below.

 ©2005 The American Physical Society

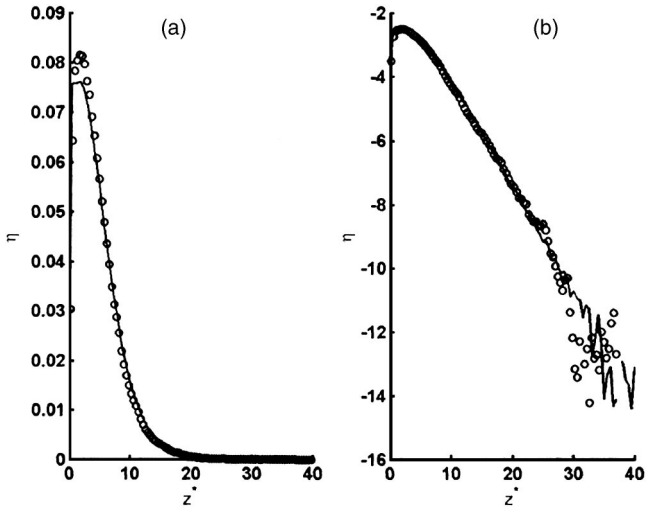

FIG. 2. A comparison of the packing fraction profile determined from molecular dynamics simulation and experiment. The symbols show the experimental packing fraction, the solid line shows the packing fraction determined by simulation, with (a) linear axes and (b) log-linear axes.

convection rolls than is possible with the outer cylinder only. In particular, for appropriate values of the coefficients of restitution, particles may move downwards near the inner cylinder and two or more toroidal rolls, with alternate directions of circulation, might form. In this article we present a systematic experimental and numerical study over a wide range of combinations of inner-wall/outer-wall coefficients of restitution to investigate this proposal.

II. GRANULAR BED AND CELL GEOMETRY

A. Numerical and experimental geometry

The experiments and the numerical simulations were both performed using an annular cylindrical geometry (see Fig. 1 for the definition of the coordinate system variables) where dissipation at the inner wall provides, compared to previous experiments [6], an additional control parameter through which the direction and magnitude of the convection rolls may be controlled.

B. Experimental procedure

The experimental cell consisted of an aluminium cylinder, of radius $R_o = 72.5$ mm, with a glass plate attached to the base to provide a low dissipation boundary for energy input. The cell was vibrated in the vertical direction using an electrodynamic shaker system, with a frequency of 50 Hz and typical amplitude of vibration, A_o of 1.24 mm. Aluminum annular inserts were placed within the cylindrical cell at a radius $R_i = 17.5$ mm, equivalent to 3.5 particle diameters. In order to minimize air drag effects, the cell was evacuated prior to each experimental run.

The grains consisted of glass ballotini beads, of diameter $\sigma = 5$ mm, with particle-particle coefficient of restitution (measured using high speed photography), $\varepsilon = 0.91$ and particle-Al wall coefficient of restitution, $\varepsilon_w = 0.79$. The

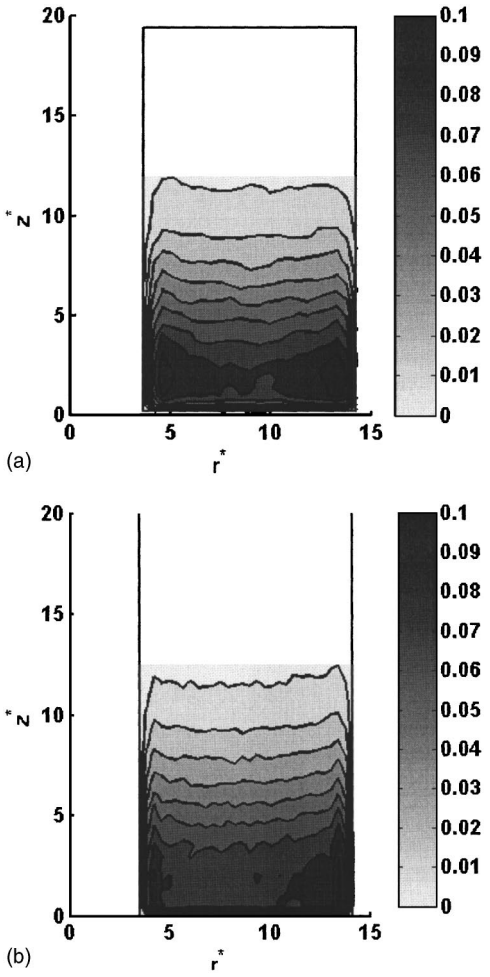

FIG. 3. Packing fraction contour plots in z-r cylindrical coordinates after averaging around the azimuthal direction: (a) experimental and (b) simulation results.

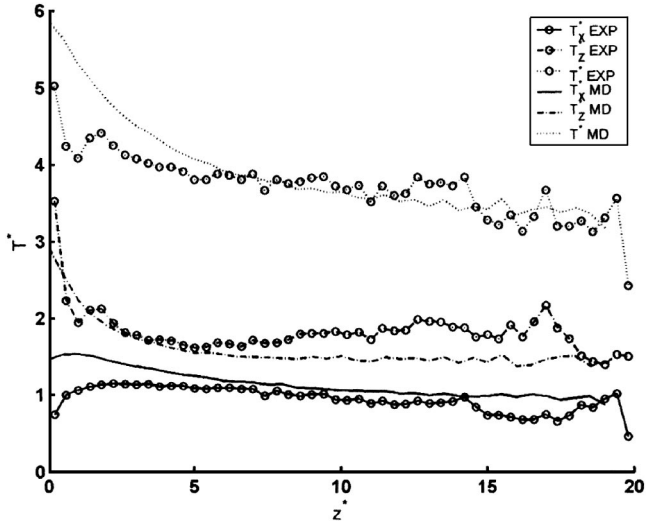

FIG. 4. Granular temperature distributions: comparison of experimental and simulation results for each component. The upper curves represent the temperature distribution $T^* = (2T_X^* + T_Z^*)$, showing how the isotropic component of the temperature behaves as a function of height.

particle-base (glass) coefficient of restitution was measured to be $\varepsilon_b = 0.91$. A single layer of random loose packed particles (total number $N = 661$) was placed within the annulus and the experimental cell vibrated to fluidize the system.

The motion of the beads in the cell was followed using positron emission particle tracking (PEPT). This radioactive-labeling technique allows for one single particle, indistinguishable from the other beads, to be tracked and its coordinates logged for periods potentially up to 6 h, though typically in this work for between 30 and 60 min. The tracer was labeled through irradiation with ^{3}He particles. The interaction between the oxygen present in the ballotini beads and the ^{3}He particles results in the formation of ^{18}F. This decays rapidly through positron emission, and considering the high probability of a collision with an electron, quickly results in annihilation and the formation of back-to-back 511 keV photons. These highly energetic γ rays are then detected simultaneously by the NaI-scintillator-based photon detectors [14]. This technique has proved to be a powerful method for investigating rapid granular flows. This is due to its high accuracy (<2 mm) and high temporal resolution ($\sim 1-2$ ms), making it suitable for tracking fast moving particles, such as those seen in granular fluidized beds [15].

C. Model and simulation

The geometry of the model system is analogous to the experimental apparatus with an annular cylindrical set up with two concentric cylinders of radii R_i and R_o. Simulations of the model were performed using an event driven procedure where particle motion is followed and time is updated at every collision between particles or between particles and one of the boundary surfaces. The equations, based on the inelastic hard sphere model, specifying the postcollisional velocities resulting from particle-base, particle-wall and particle-particle collisions are [13]:

$$\mathbf{v}_i' = \mathbf{v}_i - (1 + \varepsilon_b)[(\mathbf{v}_i - \mathbf{v}_b) \cdot \hat{\mathbf{r}}]\hat{\mathbf{r}}, \tag{1}$$

$$\mathbf{v}_i' = \mathbf{v}_i - (1 + \varepsilon_w)[\mathbf{v}_i \cdot \hat{\mathbf{r}}]\hat{\mathbf{r}}, \tag{2}$$

$$\mathbf{v}_i' = \mathbf{v}_i - \frac{(1 + \varepsilon)}{2}[(\mathbf{v}_i - \mathbf{v}_j) \cdot \hat{\mathbf{n}}]\hat{\mathbf{n}}, \tag{3a}$$

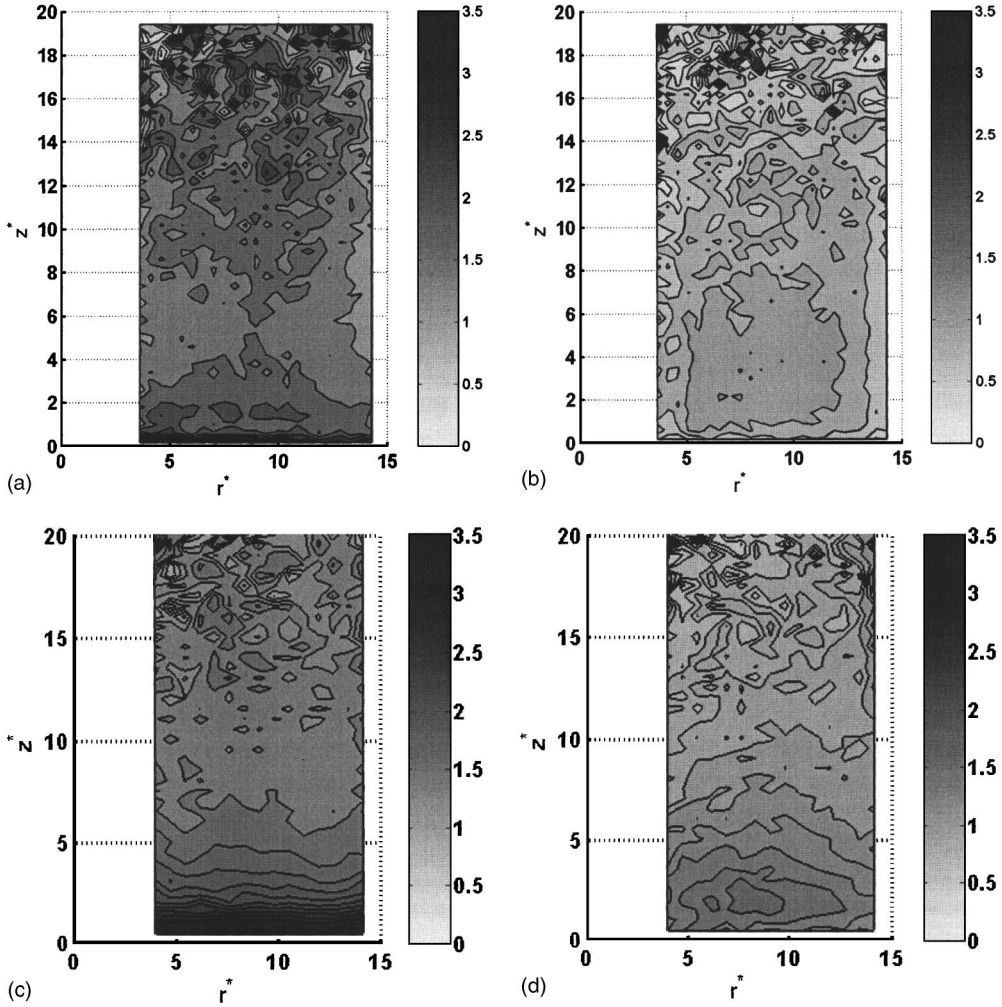

FIG. 5. Granular temperature plots in z-r cylindrical coordinates after averaging around the azimuthal direction: (a) T_Z^* from experiment; (b) T_X^* from experiment; (c) T_Z^* from simulation; (d) T_X^* from simulation.

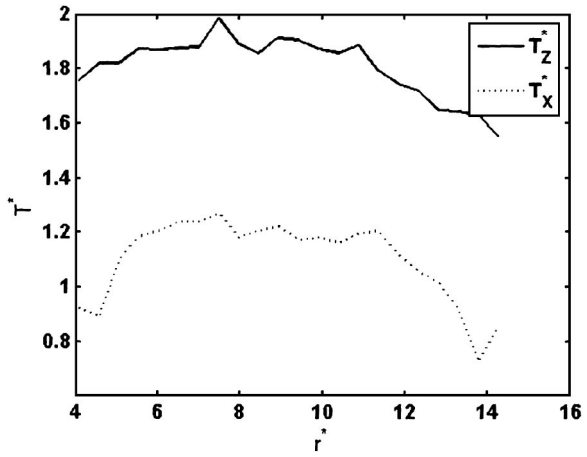

FIG. 6. Experimental radial distribution of temperature, T_Z^* and T_X^*, averaged over the range of heights 12.5 mm to 25 mm (2.5 to 5 particle diameters).

$$\mathbf{v}_j' = \mathbf{v}_j + \frac{(1+\varepsilon)}{2}[(\mathbf{v}_i - \mathbf{v}_j)\cdot\hat{\mathbf{n}}]\hat{\mathbf{n}}, \tag{3b}$$

where $\mathbf{v}$ is the velocity of a grain, the subscripts denote the grain and direction of collision, $\hat{\mathbf{n}}$ is the unit vector from the center of one of the colliding particles to that of the other, $\hat{\mathbf{r}}$ is the unit vector pointing from the center of a colliding particle and the point of impact with the base or wall and the prime denotes a postcollisional velocity. We define four coefficients of restitution to reflect the range of conditions possible: particle-particle, ε particle-wall, ε_w, where ε_{iw} and ε_{ow} are used to differentiate between the inner and outer walls, respectively; and finally the particle-base coefficient of restitution, ε_b. The grains and the walls are considered frictionless and rotational motions are not considered.

Energy is introduced into the system via the vibrating base. Experimentally, the base velocity takes a sinusoidal form, characterized in the usual way by amplitude and frequency. Numerically, however, collisions with sinusoidal vibration profiles are difficult to handle and we use a symmetric sawtooth base velocity profile. This approach is justified by the results of McNamara and Luding [16], who have shown that the symmetrical sawtooth and sinusoidal functions result in no perceivable difference in the behavior of the vibro-fluidized granular bed, apart from a scaling in the energy transferred to the bed. They proposed an empirical relationship between energy input rate and the base velocity of the bed, and characterized this using a single exponent [16]. However, as this relationship is dependent on knowing the granular temperature of the beads of the particles above the base before choosing the appropriate scaling factor, in this paper we choose the speed of vibration of the base in the MD simulation by varying the amplitude until the temperature gradient near to the base matches the experimental results. The base amplitude for the sawtooth simulation velocity profile that best matched the experimental results was $A_o = 1.12$ mm, and this amplitude was used for our initial comparison between experiment and numerical simulation (Sec. I D).

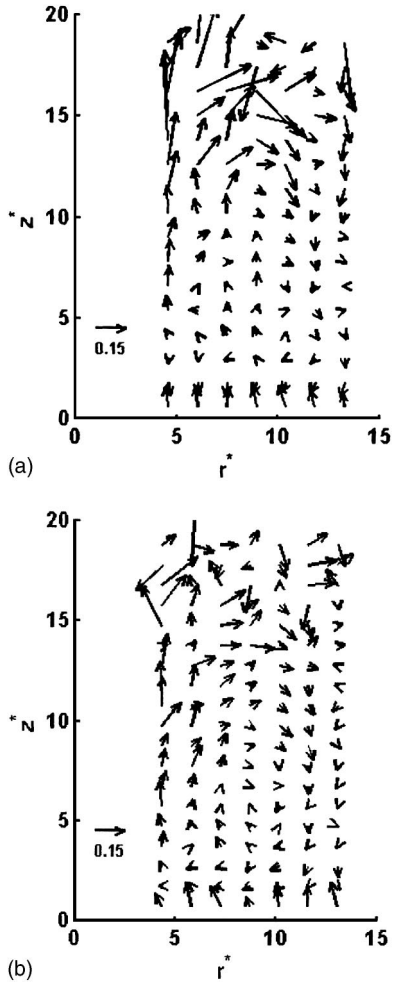

FIG. 7. Nondimensional velocity vector field from (a) experiment and (b) numerical simulation, where the nondimensional velocity, v^*, is given by $v^* = v/(g\sigma)^{1/2}$.

D. Data analysis

1. Density profiles

Experimentally the density of particles is calculated by counting the number of times the tracer particle is detected in a volume element and weighting this by the time spent in that element. Numerically, the number density, n, is determined first by summing the number of particle centres detected in a volume element and then averaging this over the course of the simulation. The number density is then converted into the packing fraction η, the ratio of the particle volume to the volume element, using $\eta = n\pi\sigma^3/6$, where σ is the particle diameter.

Figure 2(a) shows a comparison of the experimental and numerical packing fraction profiles for $N = 661$ averaged over the cross-sectional area of the cylinder, with Fig. 2(b) showing the same data on semi-log axes. In this and subsequent figures, coordinates z and r are converted to nondimensional form, denoted throughout by the superscript *, by dividing by σ. One can see that the matchup is good, with closely matching profiles. However, the zone close to the base shows some deviation. Further differences between simulation and

experiment are highlighted in Figs. 3(a) and 3(b) (showing experimental and simulation results respectively), which show contour plots of the two-dimensional packing fraction distribution on the *z*-*r* plane. A contributing cause for the differences is the spatial resolution of the PEPT facility and the associated coarsening of the data. This means that we see a decline in density as we approach very close to the wall, but in reality this is an experimental artifact due to the errors involved in locating particles [15]. Clearly, in the case of the simulations we do not suffer from such problems: the particle locations are given to an accuracy of the order of the round-off errors associated with the computer program. The simulations [Fig. 3(b)] show the clearest evidence that the number density increases substantially close to the walls. The outer wall shows the highest increase, while near to the inner wall we see a more modest rise. The smaller rise near to the inner wall can be attributed to the fact that less energy is dissipated from this region because of the smaller surface area. Therefore, unless one reduces the coefficient of restitution of the outer wall independently of that of the inner wall, one will always see a higher dissipation rate at the outer wall, and hence, a relatively higher density than at the inner wall. An additional difference is that experimentally we would expect a velocity-dependent coefficient of restitution: at low impact velocities less energy will be dissipated than at high collision velocities.

2. Granular temperature

In this paper we define the components of the granular temperature, T, in terms of the second moment of the velocity distribution:

$$T_X = \frac{1}{2}m\overline{v_X^2}, \quad T_Y = \frac{1}{2}m\overline{v_Y^2}, \quad T_Z = \frac{1}{2}m\overline{v_Z^2}, \tag{4}$$

where m is the mass of the grain, v is the grain velocity, and the subscripts x, y, and z denote the direction of the components. This is determined in experiment from the short time mean squared displacement [17], but in simulation it is calculated directly from the velocity distribution. The temperature values presented in subsequent figures were converted to nondimensional form (denoted by the superscript *) by dividing by $mg\sigma$, where g is the acceleration due to gravity.

The experimental and numerical granular temperature profiles are in reasonable agreement for $N=661$ as can be seen in Fig. 4. Figures 5(a) and 5(b) show the two-dimensional distribution of granular temperature in the z and the x directions respectively for experiment, and in Figs. 5(c) and 5(d) for numerical simulation. These results were obtained by integrating the three-dimensional distributions about the azimuthal direction to improve signal-to-noise ratio. One can see clearly that the x-direction granular temperature is lower than the z granular temperature, as one would expect. However, if we examine the granular temperatures as a function of distance from the axis of the cell, it can be observed that T_X is strongly affected by the presence of the sidewalls (Fig. 6) with decreases of over 30% compared to the central region. A small reversal in this trend for T_X immediately adjacent to each wall is an artifact of the temperature measurement procedure [15]. One can also see a reduction in the z granular temperature, but this is not as pronounced. As the collision with the wall will result predominantly in energy being lost from motion in the x direction only, one will naturally expect this reduction to be greater in the x direction than in the z direction.

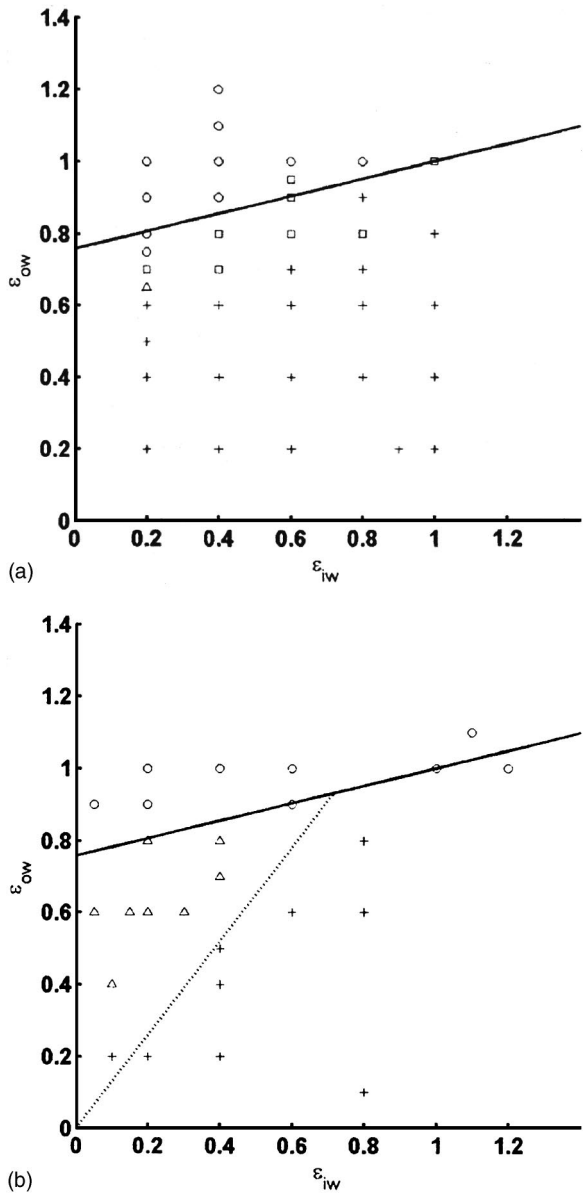

FIG. 8. Phase diagram showing the number and direction of convection rolls. Crosses indicate a single convection roll moving in a clockwise direction, circles indicate a single convection roll moving in an counterclockwise direction, triangles indicate a double convection roll and squares indicate systems where the direction of the roll was not sufficiently clear to determine the type of roll. (a) $N=661$; (b) $N=2644$.

3. Velocity fields

Figures 7(a) and 7(b) show the numerically and experimentally determined mean velocity fields for $N=661$. These were calculated by numerically differentiating the particle

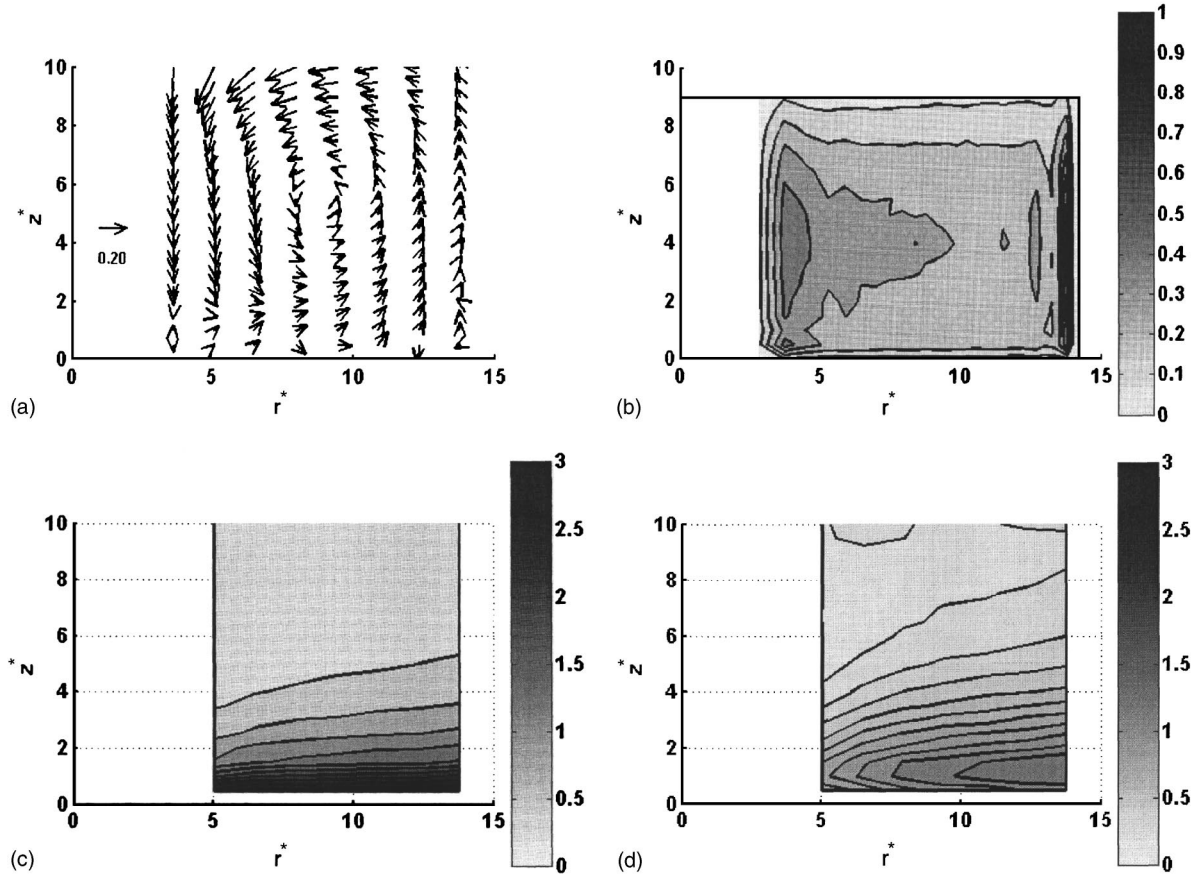

FIG. 9. An example of counterclockwise rotation produced using numerical simulation with the parameters $\varepsilon_{iw}=0.2$, $\varepsilon_{ow}=0.9$, $A_o^*=0.302$, $N=2644$, $R_i^*=3.5$, and $R_o^*=14.5$, (a) nondimensional velocity field, (b) packing fraction, and (c) and (d) granular temperature in z and x directions, respectively, rescaled for a particle diameter of 5 mm, and mass of 1.874×10^{-4} kg.

position data over 20 location events. In comparison to convection fields for cylindrical systems [9], the velocity field is not as strong. The increased density at both walls has the effect of creating competing buoyancy effects at the walls of the system, reducing the strength of the convection field. However, as we shall see in the next section, if we vary the dissipation at the inner or outer boundaries, one may induce convection rolls in one or the other or both directions. In Sec. II we will examine the phenomena observed here in more detail by performing a systematic numerical study of the system.

III. NUMERICAL INVESTIGATION OF BED BEHAVIOR

A. General behavior

Increasing the number of particles in the system can induce a convectionless system to form a convection roll, or more than one in some cases [5]. In a cylinder this usually takes the form of a single roll that moves down in the region closest to the wall and upwards at the center. It is in the region close to the wall that the system is densest and thus where the particles are pushed down. In 2D simulations, with elastic walls, the convection rolls were observed to move either clockwise or counterclockwise, with no preference in direction, when a critical level of dissipation in the system had been reached [5]. In the simple 3D system (with only an outer wall) either strong convection rolls in the clockwise sense or very weak rolls in the opposite sense were observed depending on the value of the grain-wall coefficient of restitution [13]. However, in our system, the three dimensional annular geometry means that the dissipation rates at the wall, and thus the density increase and heat flux in these regions, is also highly dependent on the difference in the surface area of the inner and outer walls. By controlling the dissipation rates at the wall and by varying the inner wall radius and the grain-wall coefficient of restitution, we can obtain some measure of control over the strength and direction of the convection rolls. As will be discussed below, one also may induce more complex convection rolls by increasing the dissipation in the system, by increasing grain-wall or grain-grain dissipation or by balancing the tendency of a roll to form in one direction or another. In this section we will first explore the behavior of the granular bed in the ε_{iw}-ε_{ow} phase space. We will discuss the appearance of the convection rolls and their relationship to the simulation parameters. Finally, we will present evidence that multiple convection rolls may be induced experimentally.

B. Convection roll phase diagrams

The control over the size and amplitude of the convection rolls enables us to explore the effect of the number of grains

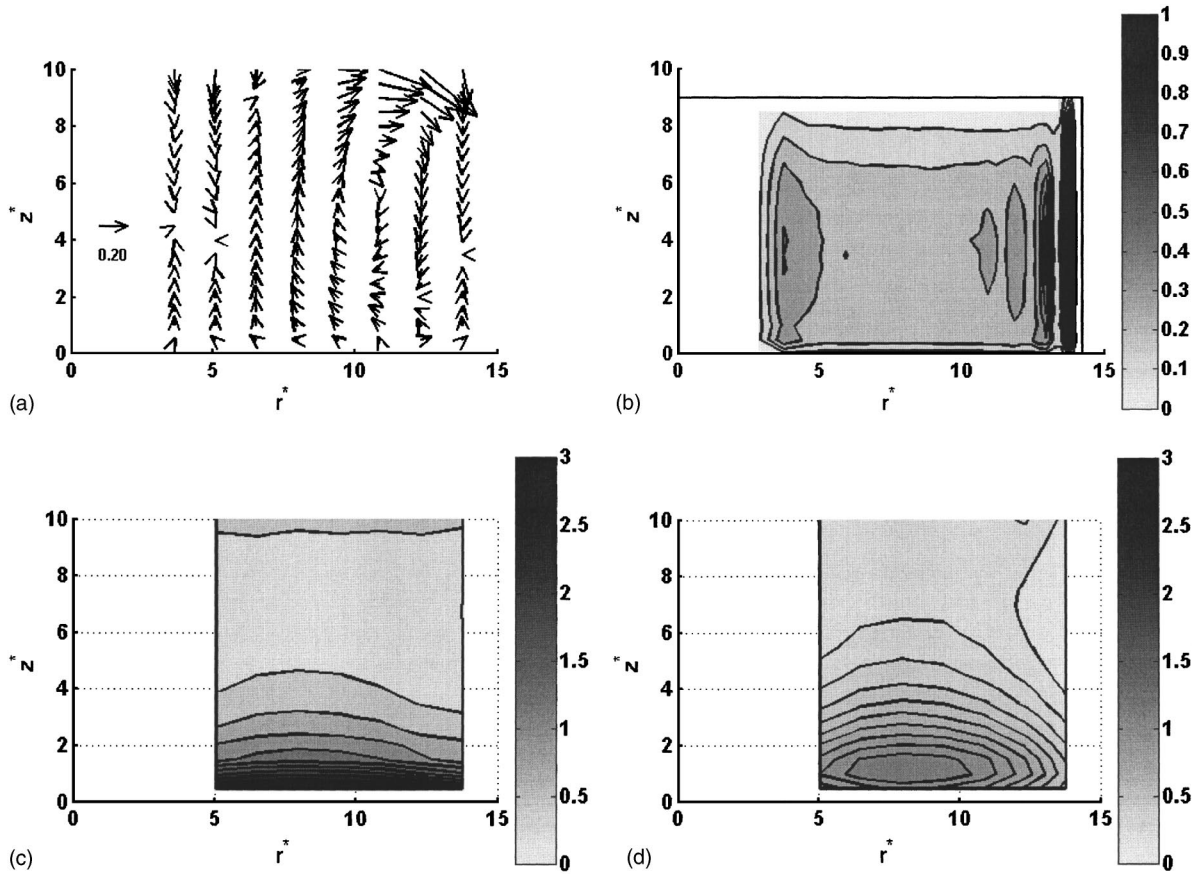

FIG. 10. An example of clockwise rotation produced using numerical simulation with the parameters $\varepsilon_{iw}=0.2$, $\varepsilon_{ow}=0.2$, $A_o^*=0.302$, $N=2644$, $R_i^*=3.5$, and $R_o^*=14.5$, (a) nondimensional velocity field, (b) packing fraction, and (c) and (d) granular temperature in z and x directions, respectively, rescaled for a particle diameter of 5 mm, and mass of 1.874×10^{-4} kg.

and the wall coefficients of restitution on convection. A number of studies have shown that the system becomes progressively less stable as the grain-grain dissipation is increased and this is observed but not explored in this paper. Ramirez *et al.* [5] define a dissipation parameter, qN, where $q=(1-\varepsilon)/2$ and show that it may be used as an order parameter describing the stability of the system. An alternative approach is taken by Khain and Meerson [7] based on hydrodynamic equations for a granular bed, but in this study we effectively vary the dissipation parameter as defined by Ramirez *et al.* [5] by varying N while keeping the grain-grain coefficient of restitution constant at $\varepsilon=0.91$, in line with experiment.

Considering first the case of low N ($N=661$, corresponding to 1 layer of beads for a geometry with inner radius, $R_i=17.5$ mm), examination of a typical velocity field and density plot shows a single toroidal convection roll with increased density regions close to the inner and outer walls. The implication of previous studies was that this increased density close to the walls was a privileged signature of a double roll, but that may not necessarily be the case for the geometry presented here.

In previous studies, the symmetry of the system has meant that there was no preferential direction to the rolls [5]. In this case, the independent control of the coefficients of restitution and geometry of the two walls suggests that certain directions may indeed be preferred. If we consider the case where the coefficients of restitution are equal, there will be significantly greater dissipation at the outer wall due to its larger surface area. A simple analysis comparing the areas of the inner and outer surfaces suggests that the dissipation will be comparable at each of the walls, assuming equal temperature and packing fraction, when the following equation is satisfied:

$$\varepsilon_{ow}=1-\frac{A_{inner}}{A_{outer}}(1-\varepsilon_{iw}). \tag{5}$$

In cases where Eq. (5) is not satisfied, we would expect the dissipation at the outer wall to dominate when the term on the left-hand side of (5) is larger than that on the right, and vice versa when the right-hand side is larger than the left.

A systematic study of the magnitude and direction of the rolls was undertaken in the ε_{iw}-ε_{ow} phase space, with parameters close to those used in the experimental study. This was performed for $R_i^*=3.5$, $\varepsilon=\varepsilon_b=0.91$, and $A_o^*=0.302$; and for two numbers of particles, $N=661$ and $N=2644$, equivalent to one and four random loose packed layers of particles, respectively. As before, the asterisk denotes a nondimensional variable where the particle diameter has been used as the scaling parameter, e.g., $R_i^*=R_i/\sigma$. The numerical simulation parameters have been chosen to be broadly those that were used in

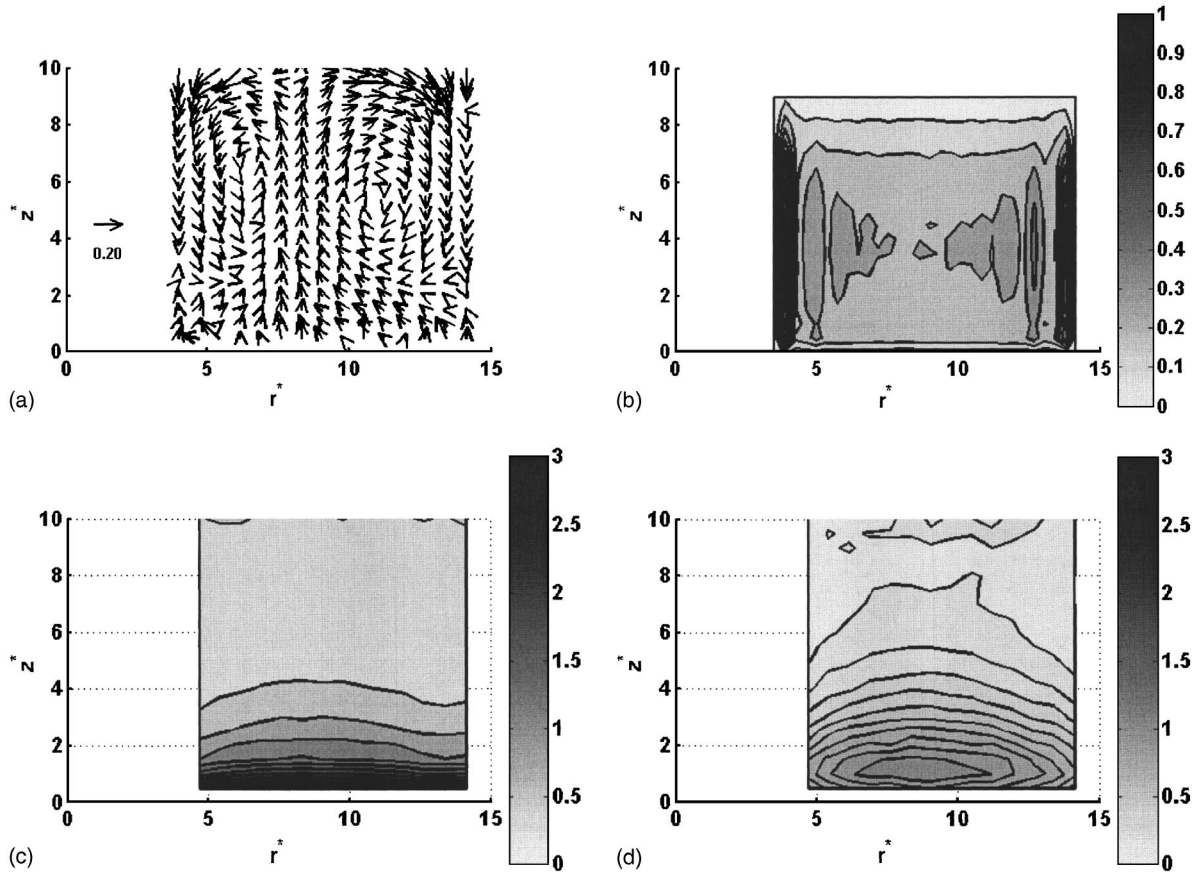

FIG. 11. An example of a double convection roll produced using numerical simulation with the parameters $\varepsilon_{iw}=0.2$, $\varepsilon_{ow}=0.6$, $A_o^*=0.302$, $N=2644$, $R_i^*=3.5$ and $R_o^*=14.5$, (a) nondimensional velocity field, (b) packing fraction, and (c) and (d) granular temperature in z and x directions, respectively, rescaled for a particle diameter of 5 mm, and mass of 1.874×10^{-4} kg.

the experiments. Figure 8(a) shows the phase diagram for $N=661$. The solid line is a representation of Eq. (5). In general, above this line we see counterclockwise motion; below it, we see clockwise rolls. There is some small variation, which may be ascribed to the geometrical properties of the wall: the outer wall is concave and acts to increase the particle collision rate compared to a flat surface, whereas the convex nature of the inner wall implies the opposite. In the case where we inject energy into the system during a collision, i.e., $\varepsilon_w>1$, the system is more stable, and although the convection rolls are still visible, they are subject to greater fluctuations and their angular velocity is smaller. Close to the situation governed by Eq. (5) we see large fluctuations in the mean velocity, and are often unable to determine the direction and number of rolls. Additionally there is a suggestion that double rolls may be present.

Figure 8(b) shows the phase diagram for $N=2644$, or 4 layers of beads. The solid line again represents Eq. (5) whereas the dashed line represents $\varepsilon_{iw}=\varepsilon_{ow}/1.3$, which is broadly representative of the boundary between counterclockwise and double roll convection. If we move along the line $\varepsilon_{iw}=0.2$ on the map in Fig. 8(b) we can go from a region where the inner wall dissipation dominates, to a region where the outer wall is dominant. When $\varepsilon_{iw}=0.2$, $\varepsilon_{ow}\approx0.3$ to 0.8, it is in between these two regimes and it appears that neither high-density region is able to control the direction of motion of the roll. This description is reflected in Figs. 9–11. The packing fraction and granular temperature distributions are also shown for comparison. The packing fractions close to one are an artefact of the high density and order present in the system; as the bin size is comparable to the particle diameter one observes regions where almost the whole measurement volume is occluded by a particle. In Figs. 9(a)–9(d) the inner wall dominates and the convection is counterclockwise in the sense of the figure. In Figs. 10(a)–10(d) the outer wall dominates and the motion is in the opposite direction. The motion in each case is clear to see. However, when $\varepsilon_{ow}=0.6$ [Figs. 11(a)–11(d)] we find that the form of the convection rolls is quite different: the grains move down at the outer wall, up in the central region, but also down near to the inner wall and we see two axially symmetric toroidal structures. This behavior suggests that not only does a double roll require high dissipation, satisfied by the high collision rate due to the large numbers of grains, but also that it requires a balance between the dissipation at the walls. If this is not the case, then the wall effects dominate and we see a single convection roll. This behavior has been seen under similar circumstances experimentally. Though further work is required to determine the exact experimental conditions under which double rolls are formed, if the experiments in Sec. I are repeated with an acetal copolymer inner wall, coated with aluminum tape ($\varepsilon_{iw}=0.62$),

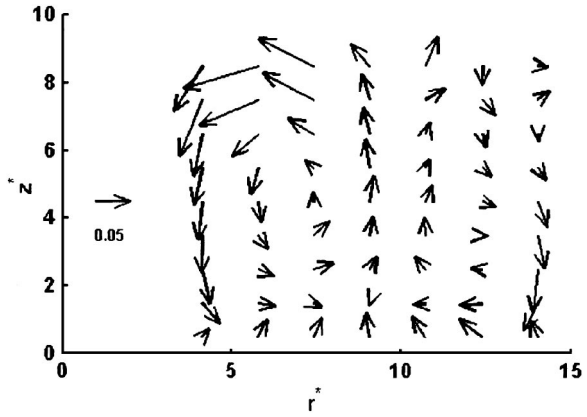

FIG. 12. Experimentally determined nondimensional velocity vector field showing evidence for double convection rolls, for $A_o = 1.24$ mm. The rolls are observed to go down at the edges and upwards in the region between the walls.

we observe the predicted form of two rolls moving downwards at the walls and upwards in the middle region (Fig. 12).

CONCLUSIONS

A comparison of numerical and experimental results for vibrated granular beds with an annular geometry showed good agreement for the granular temperature, packing fraction, and velocity fields. In the case of a monolayer of grains, higher densities and lower granular temperatures were found near both the inner and outer walls, and weak convection fields were also observed. A subsequent exploration of the ε_{iw}-ε_{ow} phase space showed that increasing the number of particles in the system could initiate strong convection currents, the direction and shape of which were dependent on the exact combination of the wall-grain coefficients of restitution. A simple model based on the respective areas and coefficients of restitution of the two walls was reasonably successful in predicting the direction of single rolls. Double convection rolls were also observed, a feature seen in recent experimental studies. Further work in this area will consider the transition from single roll convection to double roll convection, and the precise conditions under which double rolls occur.

ACKNOWLEDGMENTS

The authors would like to thank Rosa Ramirez and Pascal Viot for valuable discussions. R.D.W. performed the work as part of the EPSRC Advanced Research Fellowship scheme (GR/R75694/01) with additional support from EPSRC contract GR/N34208/01, and would like to thank Duquesne University for collaboration contributions.

[1] I. Goldhirsch, Annu. Rev. Fluid Mech. **35**, 267 (2003).
[2] J. T. Jenkins and S. B. Savage, J. Fluid Mech. **130**, 187 (1983).
[3] N. Sela and I. Goldhirsch, J. Fluid Mech. **361**, 41 (1998).
[4] J. J. Brey, M. J. Ruiz-Montero, and F. Moreno, Phys. Rev. E **63**, 061305 (2001).
[5] R. Ramirez, D. Risso, and P. Cordero, Phys. Rev. Lett. **85**, 1230 (2000).
[6] R. D. Wildman, J. M. Huntley, and D. J. Parker, Phys. Rev. Lett. **86**, 3304 (2001).
[7] E. Khain and B. Meerson, Phys. Rev. E **67**, 021306 (2003).
[8] S. Warr, J. M. Huntley, and G. T. H. Jacques, Phys. Rev. E **52**, 5583 (1995).
[9] R. D. Wildman, J. M. Huntley, and D. J. Parker, Phys. Rev. E **63**, 061311 (2001).
[10] Y. D. Lan and A. D. Rosato, Phys. Fluids **7**, 1818 (1995).
[11] E. Livne, B. Meerson, and P. V. Sasorov, Phys. Rev. E **66**, 050301 (2002).
[12] P. Sunthar and V. Kumaran, Phys. Rev. E **64**, 041303 (2001).
[13] J. Talbot and P. Viot, Phys. Rev. Lett. **89**, 064301 (2002).
[14] D. J. Parker, C. J. Broadbent, P. Fowles, M. R. Hawkesworth, and P. A. McNeil, Nucl. Instrum. Methods Phys. Res. A **326**, 592 (1993).
[15] R. D. Wildman, J. M. Huntley, J-P Hansen, D. J. Parker, and D. A. Allen, Phys. Rev. E **62**, 3826 (2000).
[16] S. McNamara and S. Luding, Phys. Rev. E **58**, 813 (1998).
[17] R. D. Wildman and J. M. Huntley, Powder Technol. **113**, 14 (2000).